Check for updates

Dynamic changes in large-scale functional connectivity prior to stimulation determine performance in a multisensory task

Edgar E. Galindo-Leon*, Karl J. Hollensteiner, Florian Pieper, Gerhard Engler, Guido Nolte and Andreas K. Engel

Department of Neurophysiology and Pathophysiology, University Medical Center Hamburg-Eppendorf, Hamburg, Germany

Complex behavior and task execution require fast changes of local activity and functional connectivity in cortical networks at multiple scales. The roles that changes of power and connectivity play during these processes are still not well understood. Here, we study how fluctuations of functional cortical coupling across different brain areas determine performance in an audiovisual, lateralized detection task in the ferret. We hypothesized that dynamic variations in the network's state determine the animals' performance. We evaluated these by quantifying changes of local power and of phase coupling across visual, auditory and parietal regions. While power for hit and miss trials showed significant differences only during stimulus and response onset, phase coupling already differed before stimulus onset. An analysis of principal components in coupling at the single-trial level during this period allowed us to reveal the subnetworks that most strongly determined performance. Whereas higher global phase coupling of visual and auditory regions to parietal cortex was predictive of task performance, a second component revealed a reduction in coupling between subnetworks of different sensory modalities, probably to allow a better detection of the unimodal signals. Furthermore, we observed that long-range coupling became more predominant during the task period compared to the pre-stimulus baseline. Taken together, our results show that fluctuations in the network state, as reflected in large-scale coupling, are key determinants of the animals' behavior.

KEYWORDS

phase, connectivity, auditory, visual, audiovisual, ECoG, ferret, cortex

Introduction

The brain continuously integrates information from different sensory systems enhancing its ability to filter noisy signals, to construct coherent percepts and guide appropriate actions (Stein and Meredith, 1993; Alais et al., 2010; Green and Angelaki, 2010; van Atteveldt et al., 2014). Such processes require the flexible and coordinated orchestration of distributed neuronal populations within and across brain areas (Singer and Gray, 1995; Engel et al., 2001; Fries, 2005; Senkowski et al., 2008; Siegel et al., 2012). Numerous studies have shown that this orchestration relies mostly on three modes of intrinsically generated coupling: synchronization of neural phase, the correlation of amplitude envelopes and the coupling between phase and amplitude (Siegel et al., 2012; Raichle, 2010; Canolty and Knight, 2010; Engel et al., 2013; Galindo-Leon et al., 2019). In addition, these coupling modes operate in multiple frequency

bands and scales, mediating different cognitive functions (Engel et al., 2001; Fries, 2005; Siegel et al., 2012; Buzsaki, 2006; Jensen and Mazaheri, 2010; Varela et al., 2001; Engel and Fries, 2010), and providing different channels for long-range communication (Bastos et al., 2015; Michalareas et al., 2016). Phase coupling, in particular, has been suggested to serve the routing of information through cortical networks and to promote selective communication between distant brain areas (Engel et al., 2001; Fries, 2005; Womelsdorf and Fries, 2007), as well as to mediate stimulus selection and prediction (Engel et al., 2001; Fries, 2005; Engel and Fries, 2010; Michalareas et al., 2016; Lima et al., 2011). However, how phase coupling supports the brain communication across scales, and how it relates to behavior, is not well understood.

A natural scenario to test the role and mechanisms of phase coupling in brain dynamics at multiple scales are multisensory tasks. In the human brain, studies of multi-scale network dynamics have remained challenging although substantial advances have been made using non-invasive methods such as EEG or MEG. In particular, only a few studies have addressed the relation between phase coupling and multisensory processing (Keil et al., 2014; Giordano et al., 2017). In animal studies, the potential role of functional connectivity involved in multisensory processing has so far been investigated only by multielectrode recordings from the same cortical areas (Lakatos et al., 2007; Kayser et al., 2008) or by simultaneous recordings from at most two different regions (Ghazanfar et al., 2008). Short-range neural interactions are well established at the level of microcircuits (Coulter et al., 2011; Bastos et al., 2012; Feldmeyer et al., 2013). Invasive studies on functional connectivity between distant population in behaving animals typically have recorded simultaneously only from relatively small numbers of sites (Womelsdorf and Fries, 2007; Gregoriou et al., 2009; Miller and Buschman, 2013; Liebe et al., 2012; Salazar et al., 2012).

Electrocorticographic (ECoG) arrays offer an option to study simultaneously the relation between multiple-scales of network dynamics and behavior (Bastos et al., 2015; Bockhorst et al., 2018; Rubehn et al., 2009; Stitt et al., 2017). Because of their bio-compatibility and recording stability, they have been used for the study of functional connectivity in networks underlying cognitive and sensorimotor functions (Crone et al., 2006; Bosman et al., 2012; Keller et al., 2014; Fukushima et al., 2015; Lewis et al., 2015) in humans (Canolty and Knight, 2010; Fox et al., 2018), monkeys (Bastos et al., 2015; Bosman et al., 2012) and rodents (Toda et al., 2018). Furthermore, small-sized ECoG electrodes can provide local information at the level of cortical columns (Bockhorst et al., 2018; Baratham et al., 2022) which, when distributed across distant regions in an array, provide a unique opportunity to study the interaction between local and global cortical dynamics.

Here, we investigated how changes in functional connectivity and power, indicative of global and local dynamics, respectively, determine the detection of multisensory stimuli. We hypothesized that in a multisensory detection task the functional coupling between modalities, rather than local power, determines the performance. We tested this hypothesis in a large-scale cortical network involving visual, auditory, somatosensory and parietal areas using a custom-made 64-channel ECoG array in behaving ferrets. Animals were trained in a 2-alternative-forced-choice paradigm to detect brief auditory and visual stimuli presented either left or right from the midline. A key finding of our study is that phase coupling of visual and

auditory regions with parietal cortex was predictive of task performance. Our results suggest that fluctuations in the networks state, particular with respect to long-range connectivity, are decisive for the response of the upcoming task during multisensory processing.

Materials and methods

Animals

All experiments were approved by the independent Hamburg state authority for animal welfare (BUG-Hamburg) and were conducted in accordance with the guidelines of the German Animal Protection Law. Data were recorded in four adult female ferrets (*Mustela putorius furo*; Euroferret, Dybbølsgade, Denmark) aged 2 and 4 years ($n = 2$ each). Animals were individually housed in standard ferret cages equipped with an enriched environment, under controlled conditions (21°C, 12-h light/dark cycle, with lights on at 8:00 a.m.). The animals had ad libitum access to food pellets, while access to tap water was restricted for 8 h prior to the experiments and training procedures. All behavioral testing was conducted during the light cycle, specifically between 10:00 a.m. and 2:00 p.m. The animals were treated with a deslorelin acetate (4.7 mg implant) chip to control their ovarian activity (Proháczik et al., 2010). Animals were trained on a two-alternative forced-choice task, described in detail below, involving lateralized detection of visual and auditory stimuli that we have established previously (Hollensteiner et al., 2015). After completion of all recording sessions (for details, see below), animals were euthanized in deep anesthesia with a lethal dose of pentobarbital (400 mg/kg i.p.). Subsequently, animals were transcardially perfused with fixative (4% paraformaldehyde in phosphate-buffered saline) and brains were removed for histological processing.

Sensory stimuli

All experiments were carried out in a dark sound-attenuated chamber (Acoustair, Moerkapelle, Netherlands). Visual and auditory stimuli were generated with the Psychophysics Toolbox (Brainard, 1997). Visual stimuli were presented on an LCD monitor (Samsung SyncMaster 2233, frame rate 100 Hz) placed 20 cm in front of the animal. Auditory stimuli were generated digitally with a sample rate of 96 kHz and delivered through two Beyerdynamic T1 speakers. Auditory stimuli consisted of white noise bursts of 100 ms duration, including 5 ms cosine rise/fall, presented with intensities between 2 and 62 dB SPL. Visual stimuli consisted of circular gratings (22.5°, 0.2 cycles/°, 5 Hz) with Michelson contrast (Cm) between 0 and 0.38. A static random noise pattern located in the center of the screen was presented to indicate trial onset by a decrease in contrast (not overall luminance). Multisensory stimuli consisted of both stimulation types presented simultaneously.

Training

Initially, ferrets were handled and accustomed to a housemade flat-bottomed tube, which served as the animals' enclosure during the experiment. Figure 1A shows a schematic of the experimental setup.

Subsequently, animals were trained in the spatial detection task, during which the unimodal as well as crossmodal psychophysical thresholds were estimated. In the task, we used a crossmodal approach that bears on established unimodal training paradigms (Nodal et al., 2008). Animals were restricted from access to water for a period of 8 h before the measurements, and conditioned by using water rewards during the task. In the first phase of the study, the animals were trained to detect unimodal auditory and visual stimuli presented in a randomized fashion. Auditory and visual unimodal detection thresholds were determined using 20 different stimulus amplitudes (auditory: 2–62 dB SPL; visual: 0–0.38 Cm) in a 1 down/3 up staircase procedure (Kaernbach, 1991). Next, unimodal and bimodal thresholds were assessed in a combined approach, using the previously determined unimodal thresholds to adjust the test parameters (for details of the procedure see Hollensteiner et al., 2015). Subsequently, the ferrets were accustomed to electrophysiological recordings during the detection task with a reduced set of stimulus amplitudes (eight per modality), adjusted to the individual psychometric functions to acquire a higher number of trials in the performance range of interest around 75% accuracy.
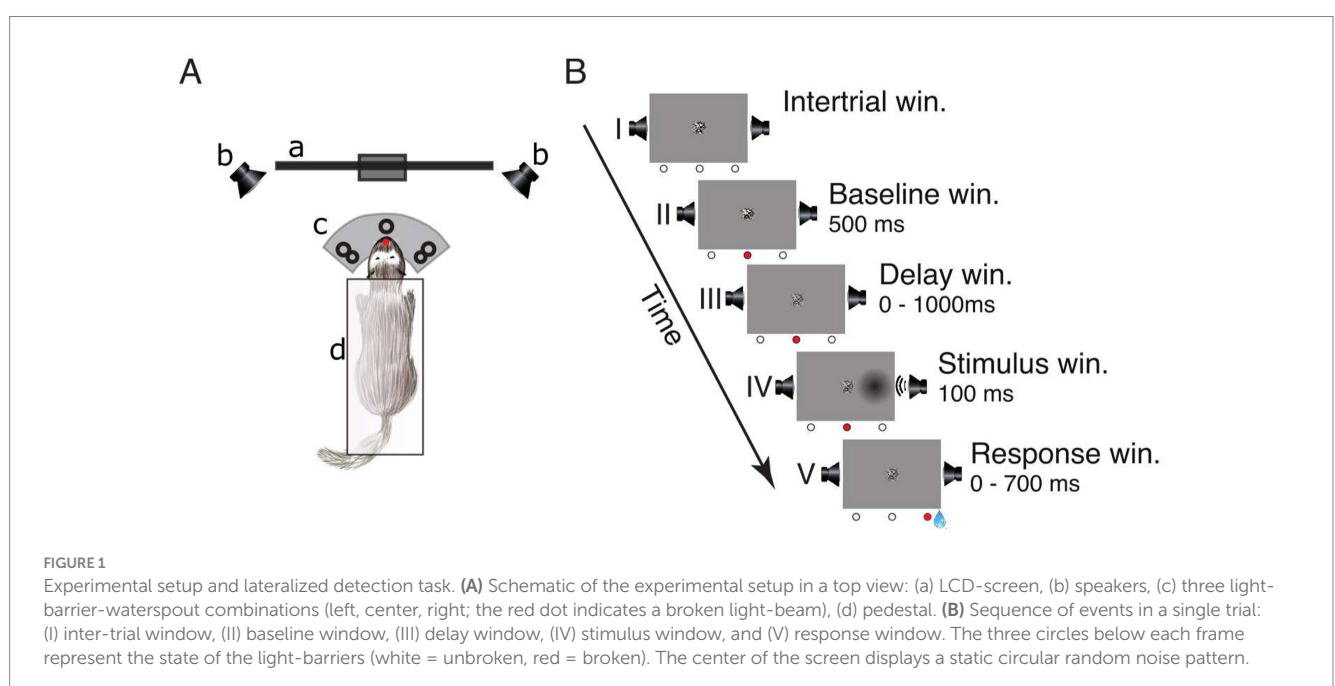
Detection task

The trial schedule of the detection task is shown in Figure 1B. To initialize a trial, the ferret had to maintain a central head position to break the central light-barrier for 500 ms. This caused the static random noise pattern in the center of the screen to decrease in contrast informing the animal that the window for stimulus presentation (from 0 to 1,000 ms after trial onset) had started. During this interval, the animal had to further maintain its central head position. A stimulus was presented for 100 ms on either the left or the right side. Stimulus presentation could be unimodal visual ("V"), unimodal auditory ("A") or a temporally congruent bimodal combination of an auditory and a visual stimulus presented on the

same side. This combination either consisted of a variable auditory stimulus accompanied by a visual stimulus of constant contrast ("Av") or, conversely, a visual stimulus of varying contrast supported by an auditory stimulus of constant amplitude ("Va"). The intensity value of the accompanying second stimulus with constant amplitude was set at a level of 75% accuracy. After stimulus offset, the animal had to respond within 700 ms by moving its head to the stimulated side; otherwise, the trial was considered as a miss (no response). If the response was correct the animal received a water reward (~80 μL) from a spout at the stimulus position and could immediately start the next trial. If the response occurred prematurely (before stimulus onset or within 100 ms after stimulus onset), was incorrect (wrong side) or omitted, the trial was immediately terminated, followed by a 2,000 ms interval during which no new trial start could be initialized.

ECoG array implantation

Micromachining technology (Rubehn et al., 2009) was used to design and implement an ECoG array that matched the anatomy of the ferret brain (Figures 2A,B). The thin-film (10 μm) polymide-foil ECoG contained 64 platinum electrodes with a diameter of 250 μm each, arranged in a hexagonal formation at an inter-electrode distance of 1.5 mm (Figures 2C,D).

The surgical procedure for the implantation of the ECoG array started with the induction of general anesthesia by using a ketamine-medetomidine mixture (10 mg/kg and 1 mg/kg, respectively). During surgery, anesthesia was maintained by ventilating the animal with isoflurane (1–1.5%) in combination with 70% N_2O and 30% O_2. To monitor the state of anesthesia, physiological parameters such as the electrocardiogram (ECG) and rectal temperature were monitored throughout the surgery. All surgical procedures were performed under sterile conditions. After the operating field was prepared, a craniotomy was performed using a saline-cooled ultrasonic microsaw (Mectron) in order to expose the posterior half of the left cerebral hemisphere.

FIGURE 1
Experimental setup and lateralized detection task. **(A)** Schematic of the experimental setup in a top view: (a) LCD-screen, (b) speakers, (c) three light-barrier-waterspout combinations (left, center, right; the red dot indicates a broken light-beam), (d) pedestal. **(B)** Sequence of events in a single trial: (I) inter-trial window, (II) baseline window, (III) delay window, (IV) stimulus window, and (V) response window. The three circles below each frame represent the state of the light-barriers (white = unbroken, red = broken). The center of the screen displays a static circular random noise pattern.
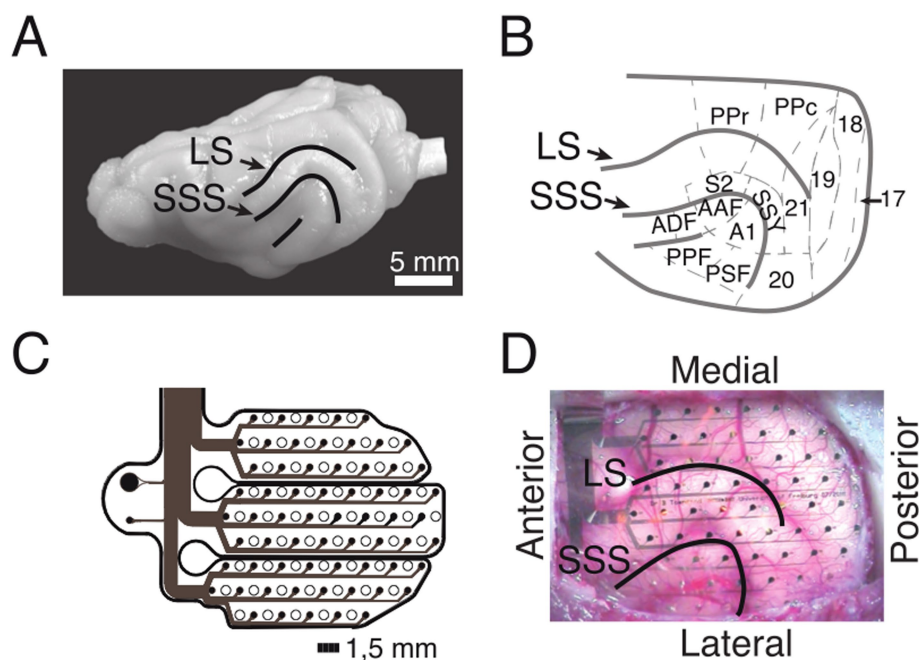
FIGURE 2
ECoG recordings from the ferret brain. **(A)** Lateral view of the left hemisphere. Lines depict sulci in the posterior part of the hemisphere. **(B)** Anatomical organization of the posterior part of the ferret brain (adopted from Bizley et al., 2007). **(C)** Schematic of the implanted ECoG (contact spacing: 1.5 mm; ø: 250 μm). **(D)** *In-situ* picture of the ECoG array over the left posterior hemisphere during implantation. LS, lateral sulcus; SSS, suprasylvian sulcus; S2, secondary somatosensory cortex; PPr/c, rostral/caudal posterior parietal cortex; 17, 18, 19, 20, 21, early and higher-order visual cortex; SSY, suprasylvian field; A1, primary auditory cortex; AAF, anterior auditory field; ADF, anterior dorsal field; PPF, posterior pseudosylvian field; PSF, posterior suprasylvian field. **(B–D)** Adapted from Stitt et al. (2017).

The dura was carefully removed and the ECoG array was gently placed on the surface of the cortex such that it covered occipital, temporal and parietal areas (Figure 2D). The dura was then folded back over the ECoG array and an absorbable artificial dura was placed above the ECoG, covering the trepanation to full extent. The excised piece of bone was fixed back in place with titanium plates and screws and subsequently the gaps were filled with fast set absorbable bone putty. Finally, the ECoG's connector was placed on top of the skull and fixed in place with titanium screws and dental acrylic. After the surgery, the animals received analgesic (carprofen, 2.5 mg/kg) and antibiotic (enrofloxacin, 5 mg/kg) medication. The animal was allowed a recovery period of a minimum of 8 weeks post-surgery. Throughout this post-operative phase, body weight and behavioral patterns were closely monitored. Regular handling sessions were maintained to ensure the animal remained habituated to the experimental setup. To align electrode positions across animals, the ECoG array placement and the cortical parcellation introduced by Bizley et al. (2007) was utilized (Figure 2B). For each animal, the exact ECoG array position over the posterior cortex was photographically documented during surgery. The locations of all 64 ECoG electrodes were then projected onto a scaled illustration of a ferret model brain. Each electrode was then mapped to the underlying cortical area.

Electrophysiological recording and preprocessing

Local field potentials (LFPs) were digitized at 1.4 kHz and sampled simultaneously with a 64-channel AlphaLab SnR recording system (Alpha Omega Engineering, Israel). The high pass filter was set at 0.1 Hz and the low pass filter at 357 Hz.

To ensure comparability across animals and modalities, only recording blocks with an accuracy of 75 ± 10% were considered in all electrophysiological analyses. Furthermore, this selection of trials ensured better comparability between all four modalities because the value that was fixed during the bimodal stimulation was set at a level of 75% accuracy for all stimulation amplitudes. To assess a sufficient amount of trials with stimulus presentation contralateral to the implanted hemisphere per modality in the 75% accuracy range, trials collected on different days were pooled; (see Hollensteiner et al., 2015) for non-stationarity effects across sessions.

All offline data analysis was performed using custom scripts in Matlab (The Mathworks Inc., MA). The hardware-filtered LFP signals were band-pass filtered with a phase-preserving fourth-order Butterworth filter between 2 and 200 Hz. Next, band-stop Butterworth filters at 49–51, 99–101 and 149–151 Hz were applied to notch the line noise. Subsequently, the continuous LFP signals were cut into epochs aligned to trial, stimulus and response onset, respectively. In each of these analysis time windows data were cut from 500 ms pre- to 500 ms post-onset, with 500 ms real data padding on each side to prevent edge artifacts in frequency space. Afterwards, we applied independent component analysis (ICA) (Hyvärinen and Oja, 2000) to the concatenated analysis window data in order to detect and remove ECG, muscle and eye blink artifacts. Next, we re-referenced the LFP time series of each ECoG contact with the LFP time series of its next posterior neighbor. This processing step created 55 virtual electrodes from the 64 recorded contacts. The new virtual electrode was located in the midpoint between both real electrode positions. Subsequently,

the oscillatory signal components of unimodal and bimodal trials were analyzed using spectral decomposition.

Spectral power analysis

Channel-wise spectral power was computed by taking the square of the absolute value of the Fourier transform. Spectra were computed for all three analysis time windows using a Hanning window approach (2–200 Hz, 2 Hz steps, 500 ms window; for the LFP spectrogram the window was shifted from –500 ms to 500 ms around the window of interest) in 1 ms steps.

Quantification of phase locking

To estimate phase synchronization between ECoG signals, we calculated the phase locking value (PLV) (Lachaux et al., 1999) across all frequencies (2–200 Hz). In general, the instantaneous phase θ was extracted from the analytic signals that were produced by the Fourier transform of the convolution of the ECoG time series with the Hanning window. The PLV between channels A and B at carrier frequency f is defined as follows (Equation 1):

$$\text{PLV}_{AB}(f) = \frac{1}{N}\left|\sum_{n=1}^{N} e^{i\left(\theta_n^A(f)-\theta_n^B(f)\right)}\right| \qquad (1)$$

For an event related paradigm the circular average of phases is in general non-vanishing, and a non-vanishing result using the classical definition of PLV does not imply statistical dependence between phases in two electrodes. Therefore, we corrected for evoked effects and defined the PLV here as Equation 2

$$\text{PLV}_{AB}(f) = \left|\left\langle e^{i\left(\theta^A(f)-\theta^B(f)\right)}\right\rangle - \left\langle e^{i\theta^A(f)}\right\rangle\left\langle e^{i\theta^B(f)}\right\rangle\right| \qquad (2)$$

where $\langle\,\rangle$ denotes average over trials. For an infinite number of trials, the PLV defined here vanishes exactly if the phase in electrode A and B are statistically independent. To contrast PLV between modalities, we first computed the global mean PLV for the same time windows selected in the spectral power analysis. Subsequently, the PLV between anatomical regions, as defined in Figure 2B, was calculated by averaging across all virtual electrodes overlaying the same area. To normalize and compare PLV values from hit and miss trials we computed the sensitivity index (d'), which is defined by Equation 3:

$$d' = \frac{\mu_{\text{hit}} - \mu_{\text{miss}}}{\sqrt{\left(\sigma_{\text{hit}}^2 + \sigma_{\text{miss}}^2\right)}} \qquad (3)$$

where μ denotes the mean and σ the standard deviation for hit and miss trials, respectively.

Principal component analysis of functional connectivity

We used a similar approach to that of Leonardi et al. (2013) to identify hidden sub-networks during the baseline period that may be associated with performance by applying principal component analysis (PCA) to trial-based connectivity matrices. To facilitate the contrast in the analysis we separated matrices in groups of hits and misses. Before applying PCA, the global mean connectivity matrix was subtracted from matrices of all trials within each group before concatenating all recording sessions. To avoid redundancy we took only the lower triangular part of each nxn connectivity matrix (excluding elements of the diagonal) and then vectorized it to obtain a vector of $n(n-1)/2$ elements. The vectors of all animals were concatenated along the trial dimension into an array of $(n-1)/2 \times T$ elements, with T being the total number of trials. PCA was then performed on the resultant matrix. Eigenvectors or principal components (PCs) can be understood as features or subnetworks that characterize the variation across the collection of correlation matrices and represent network patterns. Because these capture connectivity patterns they are also called eigenconnectivities (Leonardi et al., 2013). Finally, to reduce dimensionality and obtain the main eigenconnectivities, matrices were thresholded by the lowest and strongest 10% with respect to their mean.

Directionality analysis

To estimate the direction of causal influences we calculated the phase slope index PSI (Ψ) (Nolte et al., 2008). PSI is highly robust against false estimates caused by confounding factors of very general nature, and is defined as Equation 4:

$$\tilde{\Psi}_{ij} = \text{imag}\left(\sum_{f \in F} C_{ij}(f) C_{ij}(f + \delta f)\right) \qquad (4)$$

where $C_{ij}(f) = S_{ij}(f)/\sqrt{S_{ii}S_{jj}}$ is the complex coherency, S the cross-spectral matrix, δf the frequency resolution. F is the set of frequencies over which the slope is summed. The complex coherency C is a Hermitian matrix and consequently PSI is antisymmetric and, hence, directional. Intuitively, PSI is the slope (as a function of frequency) of the phase difference between two signals averaged within a frequency band. The slope is larger, when the time lag between the signal and the coupling increases. The sign depends on which signal is earlier. It is constructed such that it vanishes (apart from statistical fluctuations) if the observed signal is an instantaneous superposition of independent sources, and the average across frequencies is weighted with coupling strength. To normalize $\tilde{\Psi}$ we divided it by its standard deviation (Equation 5)

$$\Psi_{ij} = \frac{\tilde{\Psi}}{\text{std}\left(\tilde{\Psi}\right)} \qquad (5)$$

estimated by the jackknife method. The acquired PSI matrices were thresholded equivalently to the eigenconnectivity matrices and their sign was extracted.

Results

To investigate neural responses and task-related fluctuations of functional connectivity, we recorded local field potentials (LFPs) via 64-channel ECoG arrays chronically implanted in four adult female ferrets.

Multisensory effects on behavior

Before the electrophysiological recordings were conducted, a psychometric evaluation was performed on each animal to determine the stimulus parameters (see Methods). Figures 3A,B show examples of psychometric functions fitted to the behavioral data for the *A* and *Av*, and for the *V* and *Va* conditions, respectively. For further analysis, data were taken only from trials with stimulus intensities at threshold to allow comparisons across conditions and animals (Figures 3A,B).

Reaction times (RT) have been broadly used to quantify differences between unimodal and multisensory stimulation. A *t*-test was run to investigate the differences between bi- and unimodal conditions. Responses to bimodal stimulation were, on average, faster than those to unimodal stimulation ($p < 0.05$). To evaluate whether this effect was driven by the auditory or the visual condition, we computed a one-way analysis of variance (ANOVA) on the mean RT of each animal and condition, with sensory modality as a main factor. This revealed a main effect of condition [F (3, 12) = 5.3, $p < 0.05$], but *post hoc t*-tests only revealed significant differences between the *A*-trials and both bimodal conditions. The population averages of RTs for *Av*, *Va* and *V* were not significantly different (Figure 3C). Nevertheless, the population mean RT of *V* (0.207 s) was slightly higher than both, *Va* (0.194 s) and *Av* (0.197 s). The significant difference between the RTs in the *A* and the *Av* condition suggest a multisensory interaction effect leading to reduction in RT for the bimodal stimulation. However, our data do not suggest a substantial improvement of visual detection by a concurrent auditory stimulus.

LFP power reflects stimulus processing and response preparation

A major aim of our analysis of the electrophysiological data was to test the relation of power and functional connectivity to task performance by contrasting hit and miss trials. In the hit trial group, we included all trials with stimulus intensities around 75% threshold and stimulation contralateral to the implanted ECoG (265 ± 14 hit trials per animal). To match the number of hit trials we used all miss trials (236 ± 45 miss trials per animal) throughout all sessions (15 ± 2 sessions per animal). Miss trials were defined as those with sensory stimulation that did not elicited a behavioral response, i.e., the ferret maintained the centered head position throughout the response window. The number of false responses, i.e., orientation of the ferret to the side contralateral to the sensory stimulation, were too few and highly variable across animals (104 ± 58 false responses per animal) and, thus, were not considered for analysis of the electrophysiological data.

We checked whether the spectral characteristics of LFPs immediately before task execution predicted the animal's performance. To assess how LFP spectral characteristics evolve during hit, miss and bi- and unimodal stimulation, we computed the power across time windows aligned to baseline, stimulus presentation and response onset for each animal individually (Figure 4). Results of all animals were pooled after correction for different trial numbers. Power differences between hit and miss trials were analyzed in the theta (4–8 Hz), alpha (8–16 Hz), beta (18–24 Hz), gamma (30–80 Hz) and high-gamma (80–160 Hz) frequency band across the analysis time windows (Supplementary Table S1). In addition, one-way ANOVAs were calculated on power values within each frequency band with condition as the main factor to examine differences related to stimulus type (Supplementary Figure S1 and Supplementary Table S1).

Figure 4A illustrates the grand average spectra, while Figure 4B shows the time-frequency representation of power changes during each time window (baseline, stimulus and response onset) for both hit
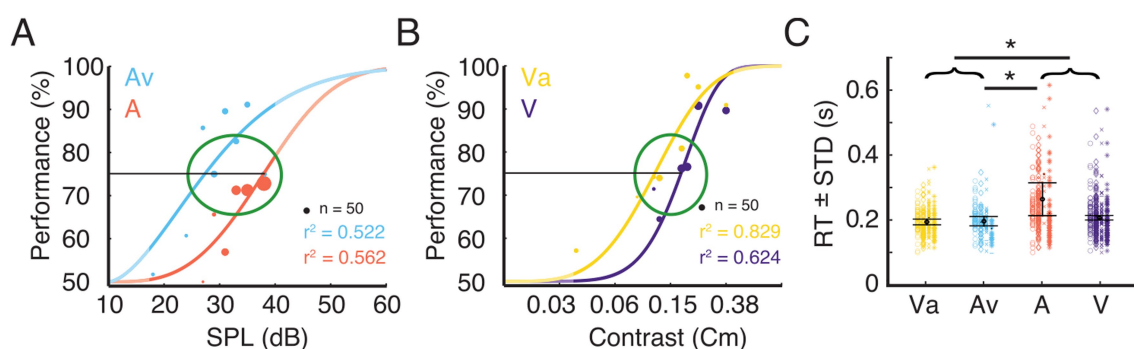

FIGURE 3
Trial selection for electrophysiological analysis and corresponding RTs. **(A)** Example data for task performance from one ferret. The plot shows psychometric functions for the uni- and bimodal condition. Stimulus response function fitted to performance data for the eight different stimulus intensities for the unimodal auditory condition (*A*) and the condition where the variable auditory stimulus was accompanied by a visual stimulus of constant contrast (*Av*). The dot diameter indicates the number of trials at a given stimulus intensity. The green ellipse indicates the stimulus intensity range around 75% performance from which trials were selected for subsequent analysis. The unmasked parts of the graphs indicate the range of the actually tested stimulus amplitudes. **(B)** Data from the same animal as shown in **A** for the unimodal visual condition (*V*) and the condition where the variable visual stimulus was accompanied by an auditory stimulus of constant intensity (*Va*). **(C)** Reaction times (mean ± standard deviation) for the four different conditions for the selected trials. The four different shapes (circle, diamond, cross, star) represent the single trial RT of each animal. Error bars indicates the mean RT ± STD across animals. Black asterisks indicate significant differences between modalities or pooled data from bimodal (*Va* and *Av*) and unimodal (*A* and *V*) stimulus pairs (brackets).
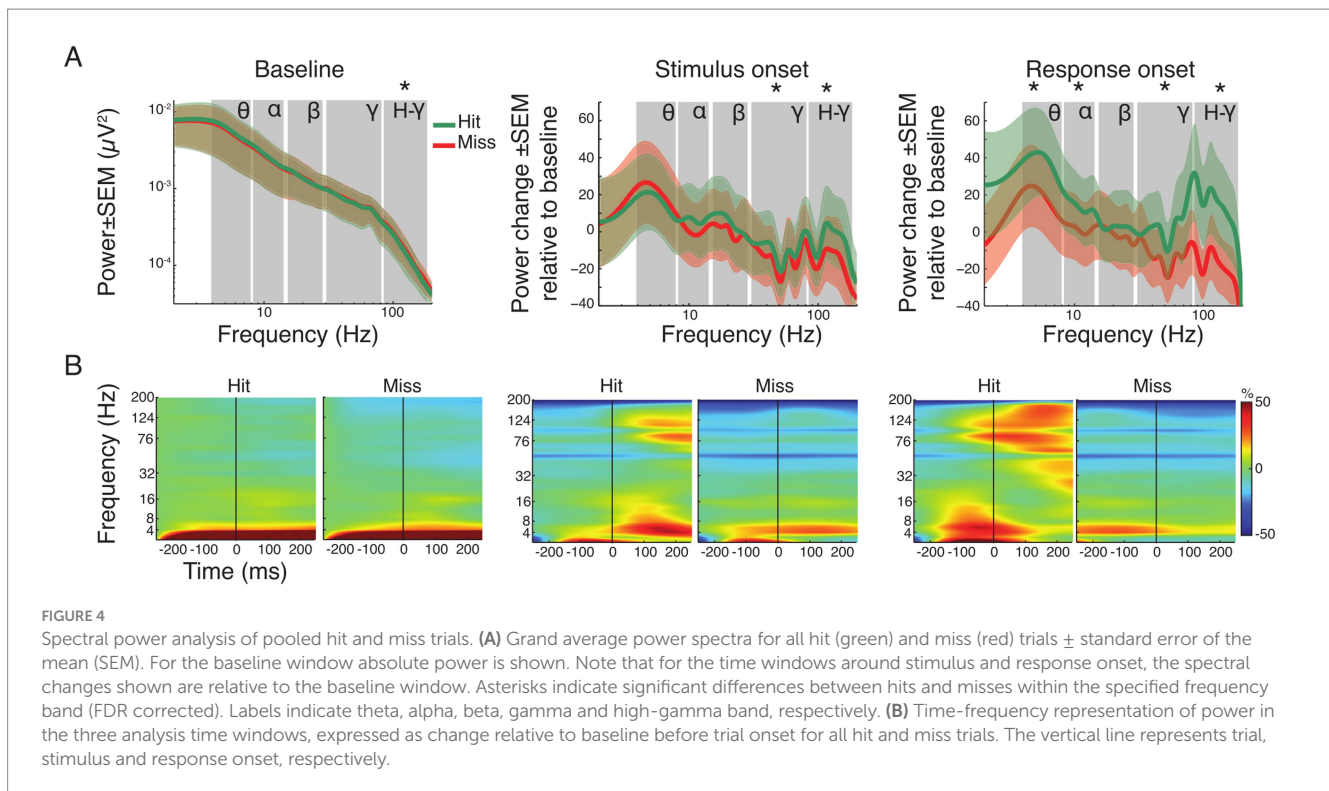
FIGURE 4
Spectral power analysis of pooled hit and miss trials. **(A)** Grand average power spectra for all hit (green) and miss (red) trials $\pm$ standard error of the mean (SEM). For the baseline window absolute power is shown. Note that for the time windows around stimulus and response onset, the spectral changes shown are relative to the baseline window. Asterisks indicate significant differences between hits and misses within the specified frequency band (FDR corrected). Labels indicate theta, alpha, beta, gamma and high-gamma band, respectively. **(B)** Time-frequency representation of power in the three analysis time windows, expressed as change relative to baseline before trial onset for all hit and miss trials. The vertical line represents trial, stimulus and response onset, respectively.

and miss trials. During the baseline, only the high-gamma frequency-band (80–160 Hz) showed moderated but significant differences, with higher power for miss trials ($p < 0.05$; FDR corrected). Comparison of the average spectra in the stimulus onset analysis window showed significant reductions for hit and miss trials in the gamma frequency-range (30–160 Hz) compared to baseline (Supplementary Table S1). However, hit trials showed significantly higher power compared to miss trials after stimulus onset in both gamma ($p < 0.001$) and high-gamma ($p < 0.001$) frequency bands (Figure 4A). Around response onset, hit trials consistently showed significantly higher power compared to miss trials in the theta- ($p < 0.01$), alpha- ($p < 0.01$), gamma- ($p < 0.001$) and high-gamma band ($p < 0.001$). Statistical comparison across time windows within hit- and miss-trials revealed significant decrease and increase in the gamma frequency range compared to baseline and stimulus onset, respectively (Supplementary Table S1; all p-values, within and across windows of interest, FDR corrected).

Supplementary Figure S2 shows the topographies of the respective spectral differences between hit and miss trials. In the baseline window, power topographies showed high spatial uniformity across all frequency bands. Around stimulus onset, notable differences occurred mainly in the beta band where, in hit trials, higher beta power differences occurred in parietal areas. The highest regional differences occurred in the response window. Occipital regions exhibited higher power across all frequency bands during response onset in miss trials compared to hit trials. In contrast, auditory and parietal areas showed increased power in lower frequency bands (theta and alpha) for hit trials. An increase of gamma band power occurred in the response window for hit trials in regions around the lateral sulcus (Supplementary Figure S2).

To investigate stimulus-type dependent effects within hit-trials a one-way ANOVA between the four conditions (*Av*, *Va*, *A* and *V*;

Supplementary Figure S1 and Supplementary Table S1) was calculated. It showed no main effect in the factor condition across frequency bands during baseline, stimulus or response onset. This suggests that power changes related to stimulus processing and response preparation did not depend on the modality of the presented stimulus or on crossmodal interactions.

Functional connectivity predicts performance

To determine whether functional connectivity predicts the animals' performance we computed the PLV between all pairs of ECoG channels for the different frequency bands. PLV analysis corrected for evoked effects was performed for the same time windows as the power analysis: aligned to baseline, stimulus and response onset. Figure 5 displays the population average PLV spectra for all hit and miss trials as well as the difference between hits and misses (Figure 5B) and the relative spectral changes in the stimulus and response onset window relative to baseline (Figure 5B). Paired *t*-tests were applied between hit and miss trials within and across all time windows for each frequency band separately. Within each analysis window, significantly higher PLV was observed for hits compared to miss trials in all frequency bands, with exception of the theta band during response onset ($p < 0.05$, FDR corrected; Figure 5A).

When compared to the baseline time window, PLV was significantly reduced in the stimulus and response onset windows in nearly all frequency bands. Exceptions were in the theta frequency band for miss trials around stimulus as well as response onset.

A one-way ANOVA within analysis time windows and frequency bands with stimulus condition as the main factor revealed significant differences in PLV between stimulation conditions (*Av*, *Va*, *A* and *V*;
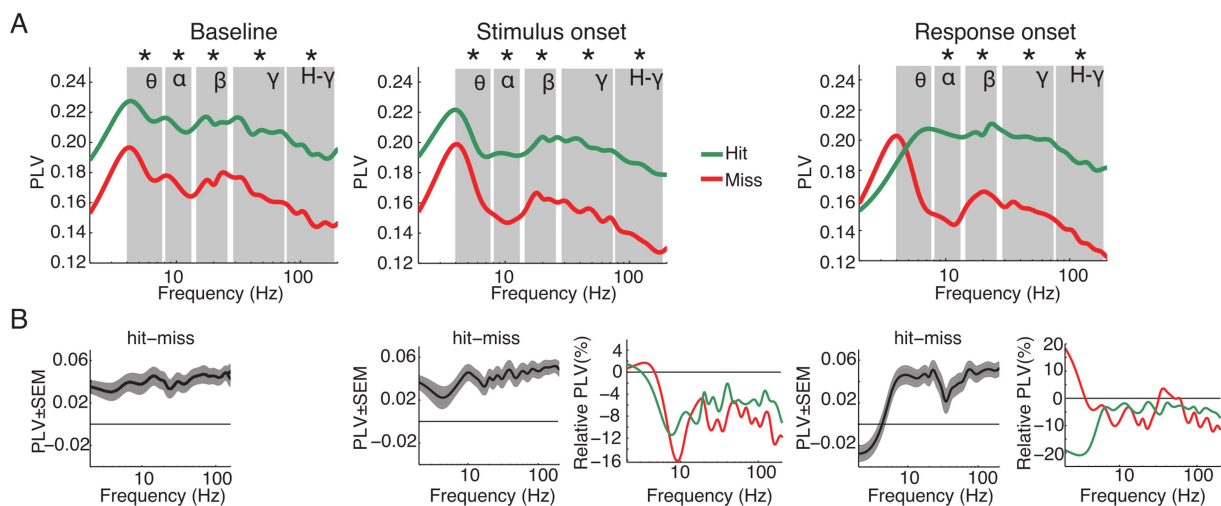
FIGURE 5
Grand average of functional connectivity for hit and miss trials. **(A)** Grand average phase locking value (PLV) for all hit (green) and miss (red) trials for the analysis time windows (baseline, stimulus and response onset). **(B)** Differences between hits and misses for the three analysis windows and changes of PLV around stimulus and response onset, expressed as changes relative to the baseline window. Asterisks indicate significant differences between hits and misses within the specified frequency band ($p < 0.05$, FDR corrected). Labels in **A** denote theta, alpha, beta, gamma and high-gamma band, respectively.

Supplementary Figure S3). During the baseline period there were no significant effects in the main factor condition in the theta frequency band [$F(3, 44) = 2.46$, $p > 0.05$]. However, starting with the alpha [$F(3, 76) = 4.98$, $p = 0.003$], beta [$F(3, 60) = 3.71$, $p = 0.016$], gamma [$F(3, 412) = 31.89$, $p < 0.001$] and high-gamma [$F(3, 652) = 56.99$, $p < 0.001$] frequency bands, there was a main effect of conditions. This effect persisted also for the windows around stimulus onset [theta: $F(3, 44) = 1.23$, $p > 0.05$; alpha: $F(3, 76) = 3.74$, $p = 0.015$; beta: $F(3, 60) = 3.5$, $p = 0.021$; gamma: $F(3, 412) = 26.12$, $p < 0.001$; high-gamma: $F(3, 652) = 55.67$, $p < 0.001$] and response onset [theta: $F(3, 44) = 2.31$, $p > 0.05$; alpha: $F(3, 76) = 3.63$, $p = 0.017$; beta: $F(3, 60) = 3.67$, $p = 0.017$; gamma: $F(3, 412) = 25.12$, $p < 0.001$; high-gamma: $F(3, 652) = 51.24$, $p < 0.001$]. Furthermore, post-hoc t-test confirmed a constant pattern of significant differences between conditions (Supplementary Table S2). In particular, for hit trials connectivity was higher in the *A* and *Av* conditions than in the *V* condition, and there was a trend for connectivity in bimodal *Va* trials to be higher than in unimodal *V* trials (Supplementary Figure S3).

Taken together, in contrast to the power, the PLV revealed significant differences between hit and miss trials. These differences occurred over a broad range of frequencies across all analysis time windows. These results suggest that large-scale phase-fluctuations in network state are determinant to the animals' performance.

Large-scale coupling shows specific changes during the task

To examine functional connectivity in relation to the topography of cortical areas, we assigned the data of each ECoG contact to a distinct region based on the functional map of cortical areas from Bizley et al. (2007) (see Methods) and constructed functional connectivity matrices accordingly (Figure 6). Cortical areas were grouped in three functional systems, comprising visual (areas 17, 18,

19, 20, 21), auditory (areas A1, AAF, ADF, PPF and PSF), and parietal areas (SSY, PPc, PPr, S2). Differences between hit and miss trials were expressed using the sensitivity index (d').
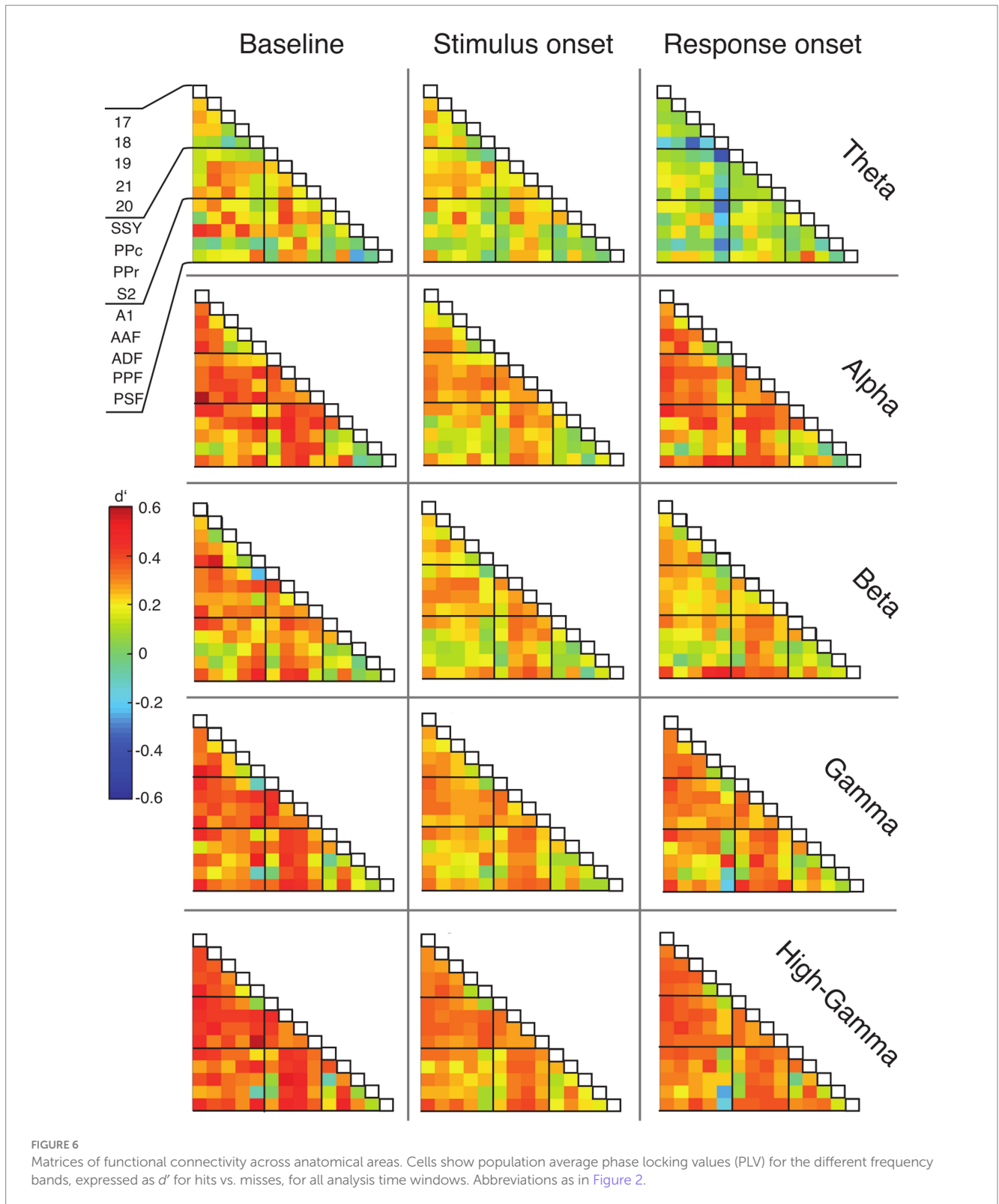
In line with the grand average PLV results, the connectivity matrices generally displayed positive d' values and, thus, higher functional connectivity for hit compared to miss trials (Figure 6). This effect was most prominent during the baseline window and decreased during the stimulus presentation. For the alpha, gamma and high-gamma band, the PLV difference between hit and miss trials increased again in the response window. Generally, connections between early sensory cortices and parietal cortex displayed the highest differences between hit and miss trials, in particular during the baseline window (Figure 6; Supplementary Figure S5).

Eigenconnectivity reveals subnetworks related to performance

We asked whether the trial-to-trial fluctuations in functional connectivity during the baseline period could affect the animal's performance. We first identified the subnetworks that most strongly contributed to fluctuations during the baseline across trials. To find the intrinsic structure in the patterns of connectivity, we applied principal component analysis (PCA) to functional connectivity matrices for hits and misses along the trial dimension (see Methods). We focused on a subset of areas (18, 19, 21, PPc, PPr, A1, and AAF) from the recorded functional systems for the analysis of task-related subnetworks to reduce dimensionality.
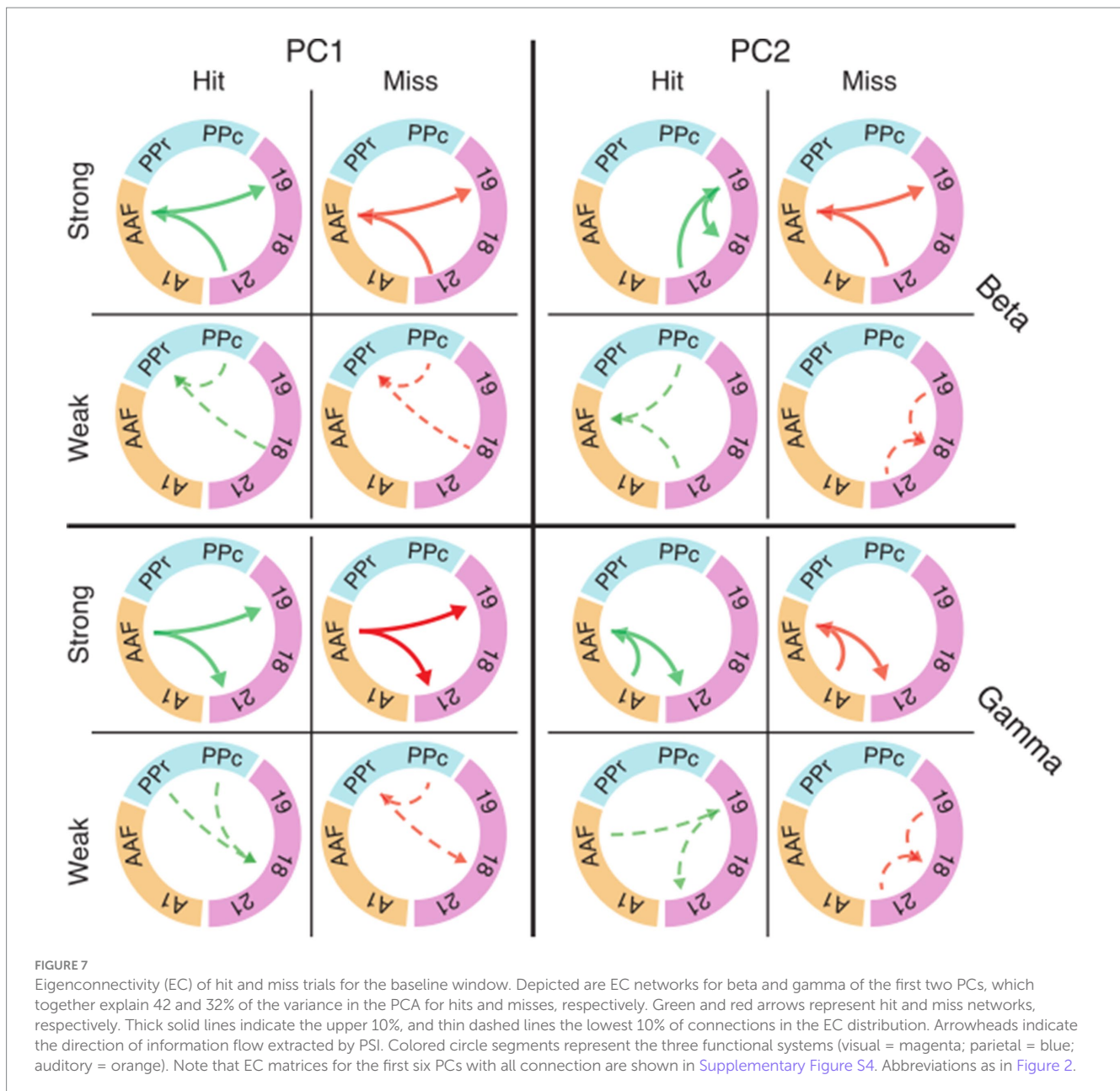
Figure 7 shows eigenconnectivity patterns in the beta and gamma bands for hit and miss trials in the first and second PCs. Only those connections which had the smallest and the largest fluctuations of functional connectivity in the baseline window are displayed (complete matrices and explained variance for PCs 1–6 in all frequency bands are shown in Supplementary Figure S4). PC1 did

FIGURE 6
Matrices of functional connectivity across anatomical areas. Cells show population average phase locking values (PLV) for the different frequency bands, expressed as *d'* for hits vs. misses, for all analysis time windows. Abbreviations as in Figure 2.

not show substantial differences between hits and misses (Figure 7A; Supplementary Figure S4). For both hits and misses, the first PC revealed that the largest fluctuations occurred between auditory and visual areas, and the smallest between visual and parietal cortices. Importantly, PC2 revealed substantial differences between hit and miss trials. These differences were most prominent in the theta,

alpha, and beta bands, but also occurred in the gamma band (Figure 7B; Supplementary Figure S4). In the beta band, a higher fluctuation in functional connectivity between AAF and visual areas was a common pattern in miss trials for PC2. A similar pattern was shown in the gamma band (Figure 7). In contrast, the highest connectivity fluctuations in the beta band for hits were observed

FIGURE 7
Eigenconnectivity (EC) of hit and miss trials for the baseline window. Depicted are EC networks for beta and gamma of the first two PCs, which together explain 42 and 32% of the variance in the PCA for hits and misses, respectively. Green and red arrows represent hit and miss networks, respectively. Thick solid lines indicate the upper 10%, and thin dashed lines the lowest 10% of connections in the EC distribution. Arrowheads indicate the direction of information flow extracted by PSI. Colored circle segments represent the three functional systems (visual = magenta; parietal = blue; auditory = orange). Note that EC matrices for the first six PCs with all connection are shown in Supplementary Figure S4. Abbreviations as in Figure 2.
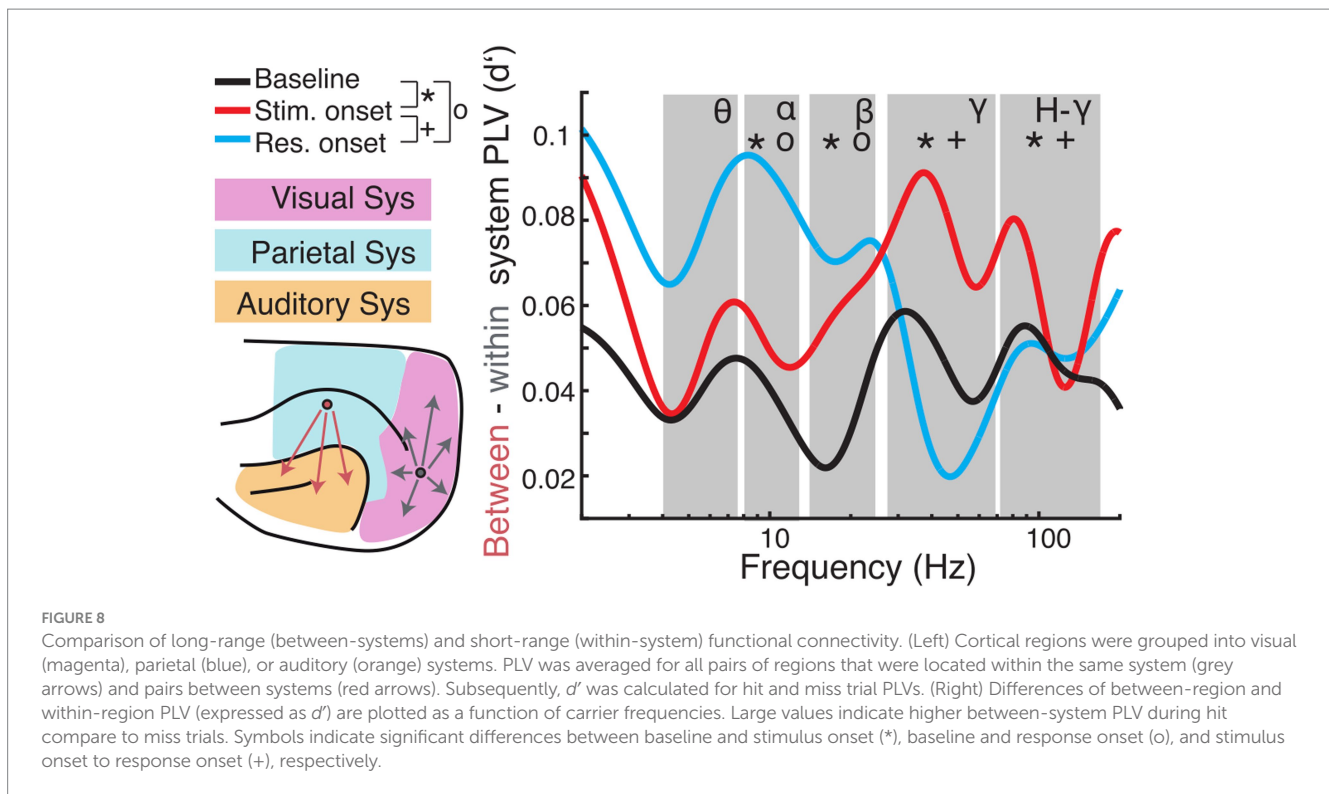
within the visual system. From the third to the sixth components, the connectivity fluctuations revealed more complex patterns, with increases as well as decreases in both hit and miss trials (Supplementary Figure S4). The directionality in Figure 7 and Supplementary Figure S4, which was extracted from PSI matrices, represents the directionality of the coupling in subnetworks and does not necessarily carry information about directionality of the fluctuation.

It should be noted that the eigenconnectivity patterns cannot be directly compared to the global connectivity differences between hits and misses described in the preceding sections because they reflect changes in subnetworks, relative to the average network coupling strength, in the two groups of trials. Importantly, our analysis shows that changes in connectivity do not occur arbitrarily across the network, but are distributed in subnetworks that show specific increases or decreases in phase coupling.

Between- and within-system interactions differ in their relation to behavior

The topography of functional connectivity changes was further analyzed by contrasting between-system and within-system interactions (Figure 8; Supplementary Figure S5). A previous study from our group showed that this is a suitable classification to determine global/local effects associated to changes in brain state (Stitt et al., 2017). For hit trials, interactions between the three functional systems were, on average, stronger than functional connections within the respective system. Regarding the within-system connectivity, the auditory system showed the lowest d'. In the period from baseline to stimulus onset, the strength of d' decreased across all frequency bands. With response onset the spectral profile of d' became more heterogeneous. In the theta-band d' decreased further, whereas it remained unaltered in the

FIGURE 8
Comparison of long-range (between-systems) and short-range (within-system) functional connectivity. (Left) Cortical regions were grouped into visual (magenta), parietal (blue), or auditory (orange) systems. PLV was averaged for all pairs of regions that were located within the same system (grey arrows) and pairs between systems (red arrows). Subsequently, d' was calculated for hit and miss trial PLVs. (Right) Differences of between-region and within-region PLV (expressed as d') are plotted as a function of carrier frequencies. Large values indicate higher between-system PLV during hit compare to miss trials. Symbols indicate significant differences between baseline and stimulus onset (*), baseline and response onset (o), and stimulus onset to response onset (+), respectively.

beta-band, and increased in the alpha-, gamma- and high-gamma band.

For statistical analysis, we averaged PLV d' values and derived the difference of d' values between long-range (between-system) and short-range (within-system) connectivity and calculated statistics across analysis time windows for each frequency band (Figure 8; for statistics across systems and within analysis time windows and frequency see Supplementary Figure S5; for condition specific statistics see Supplementary Figure S6). To reveal dynamic effects within frequency bands of interest a one-way ANOVA with time window as the main factor was computed. There was no main effect in the theta band [$F (2, 6) = 4.39$, $p > 0.05$]. The ANOVA exposed significant effects for the main factor time window alpha [$F (2, 12) = 17.17$, $p < 0.001$]; beta [$F (2, 9) = 14.43$, $p = 0.002$]; gamma [$F (2, 75) = 3.71$, $p < 0.001$]; high-gamma [$F (2, 120) = 17.94$, $p < 0.001$]. *Post hoc* t-tests revealed significant differences between baseline and stimulus onset for all frequency bands with the main effect (alpha: $p = 0.011$; beta: $p = 0.002$; gamma: $p < 0.001$; high-gamma: $p < 0.001$), between stimulus and response onset for the gamma frequency range (gamma: $p = 0.009$; high-gamma: $p < 0.001$) and between baseline and response onset in the alpha- ($p < 0.001$) and beta- ($p = 0.006$) frequency bands (Bonferroni corrected).

Overall, comparison of functional connectivity between and within cortical systems across the different analysis time windows revealed that between- compared to within-system connectivity was stronger during the task period compared to the pre-stimulus baseline. In hit-trials, phase coupling was higher between systems in the gamma frequency range during stimulus onset compared to baseline and response onset. Furthermore, low frequency (alpha and beta) coupling between systems increased around response onset in hit trials compared to miss trials. These results suggest that fluctuations in the network state, particularly with respect to long-range connectivity, are related to task performance.

Discussion

This study has aimed at investigating the cortical network dynamics at multiple spatial scales and subnetworks. We hypothesized that in tasks that involve multiple distant modalities the functional connectivity, rather than the local activity, becomes a main determinant for performance. We addressed this question in an audiovisual detection task in ferrets. We used an ECoG approach to record a large-scale network comprising visual, auditory, somatosensory and parietal areas in behaving animals over extended time periods.

In line with our hypothesis, our data show that pre-trial baseline connectivity predicts the animals' performance, suggesting that fluctuations in coupling across the network lead to variability in behavior. In contrast, mean power in the pre-trial baseline was not associated to performance. Analysis of the topography of connectivity differences between hits and misses revealed specific patterns, reflecting different functional subnetworks, associated to the response. In particular, higher global phase coupling of visual and auditory regions to parietal cortex was predictive of task performance, yet a reduction in connectivity in certain subnetworks may be necessary for distinct functional systems to detect stimuli appropriately. We also observed that long-range coupling became more predominant during the task period compared to the pre-stimulus baseline and changed its spectral profile over the course of the trials.

Relating large-scale connectivity to task performance

Among the established functional connectivity measures, coherence, in particular, has been associated to cognitive tasks in humans involving perceptual selection (Hipp et al., 2011), attentional

selection (Michalareas et al., 2016; Siegel et al., 2008), working memory (Brookes et al., 2011) or speech processing (Giordano et al., 2017; Giraud and Poeppel, 2012). Animal studies have demonstrated a relation of long-range phase coupling in various frequency ranges to sensorimotor processing, attentional selection and working memory (Bastos et al., 2015; Gregoriou et al., 2009; Liebe et al., 2012; Salazar et al., 2012; Bosman et al., 2012; Bernasconi et al., 2000; Roelfsema et al., 1997; Saalmann et al., 2012).

We found that phase coupling, in contrast to local power, differed already between hit and miss trials in the pre-trial baseline. The data indicate that stronger phase coupling in the network may lead to higher efficiency of stimulus processing and response preparation. This is in line with earlier studies that have demonstrated that increased synchrony enhances communication across brain areas [e.g., in the context of attention (Fries, 2005; Bosman et al., 2012)] supporting the role of functional connectivity in linking task-relevant modalities to areas involved in selection of responses (Siegel et al., 2012; Miller and Buschman, 2013). Indeed, we find that stronger phase coupling of early sensory to parietal areas was predictive of task performance.

Contrary to earlier studies, our results appear not to correspond to the typical vigilance- or attention-related signatures in pre-stimulus functional connectivity characterized by increases in high frequency and decreases in low frequency bands (Bosman et al., 2012; Siegel et al., 2008; Hanslmayr et al., 2007). Although the average connectivity differences between hits and misses had a rather broad spectral profile, analysis of the ratio between long-range (between cortical systems) and local interactions (within cortical systems) revealed spectral shifts in this ratio between the task period and the pre-stimulus baseline. This result highlights the role of within-area high-frequency coupling during stimulus processing, which may reflect stronger bottom-up signaling. This could relate to attentional gating, allowing relevant information to pass through the network to higher areas. In contrast, the predominance of low-frequency interactions in the epoch around response onset might indicate stronger top-down information flow (Bastos et al., 2015). Alternatively, in that interval of the trial, parts of the network could already return to a default state dominated by low frequency oscillations. Averaged across areas, spectral differences between connections with dominant bottom-up and top-down information flows, might level out and, thus, yield the broad spectral profile of connectivity changes observed in the present analysis.

Functional connectivity and multisensory processing

As discussed above, dynamic functional coupling likely constitutes a mechanism for integration of distributed neural signals and sensory systems (Singer and Gray, 1995; Engel et al., 2001; Fries, 2005; Arnal et al., 2015; Ploner et al., 2017). It has been suggested that similar mechanisms might operate for the integration of information across different sensory systems. Thus, multisensory interactions might involve dynamic coupling of oscillatory signals arising in different cortical systems (Senkowski et al., 2008; Talsma et al., 2010). In the human brain, the vast majority of studies on neural oscillations and crossmodal processing have focused on local power changes, and only few investigations have addressed the relation between multisensory processing and functional coupling (Keil et al., 2014; Giordano et al., 2017). Using a data-driven approach for analysis of functional

coupling in the human EEG, we could recently demonstrate that coherence in networks involving parietal and sensorimotor areas predicts performance in a visuotactile matching task (Wang et al., 2019). Simultaneous recordings from auditory cortex and superior temporal sulcus in the monkey have revealed increased coherence during congruent auditory and visual stimulation (Ghazanfar et al., 2008; Maier et al., 2008). While these in-vivo studies investigated multisensory interactions only by recordings from the same cortical areas or by simultaneous recordings from at most two different regions, our study has addressed multisensory networks at a larger scale involving visual, auditory and parietal cortical regions. While our data clearly demonstrate a relation of functional connectivity to task performance, we did not obtain evidence for stimulus-specific changes of coupling between visual and auditory areas, resembling recent results in anesthetized ferrets (Galindo-Leon et al., 2019), where modification of coupling structure occurred only on longer time scales and not in a stimulus-related manner.

The absence of profound connectivity effects related to multisensory interaction may relate to the nature of the task used in our study, which did not require integration of features across modalities, but only the rapid detection of highly transient stimuli. Nonetheless, our results on connectivity data support the notion that significant functional coupling can occur already between early sensory areas, suggesting that multisensory integration can already occur at early processing stages and does not solely rely on binding of information at higher processing levels (Senkowski et al., 2008; Lakatos et al., 2007; Bizley et al., 2007). This is in line with anatomical data suggesting that direct projections from primary auditory to visual cortices can enable functional coupling supporting early multisensory interactions (Bizley et al., 2015).

Network state and behavioral variability

A key result of our study is that phase coupling differed between hit and miss trials already in ongoing activity in the baseline period. The local power in this period did not differ between hits and misses. Our data suggest that fluctuations in the network state occur which lead to variability in the animals' behavior, and that these state changes are primarily reflected in shifts of long-range connectivity, rather than changes in the dynamics of local populations. Early studies assumed that ongoing neural activity corresponds to noise resulting from random signal fluctuations without any functional relevance (Zohary et al., 1994; Shadlen et al., 1996). However, this view has been challenged by evidence showing that ongoing activity carries information that can shape sensory and cognitive processing (Engel et al., 2001; Galindo-Leon et al., 2019; Keil et al., 2014; Arieli et al., 1996; Fries et al., 2001; Busch et al., 2009). Such fluctuations of ongoing activity do not occur only locally, but are strongly synchronized across spatially distributed neuronal populations (Galindo-Leon et al., 2019; Stitt et al., 2017; Steriade et al., 1996; Fischer et al., 2018).

Phase coupling of oscillations in pre-stimulus epochs has been shown both in animal and human studies to predict perception and performance in cognitive tasks. For instance, studies in monkey visual cortex indicate that fluctuations in gamma-band phase coupling modulate the speed at which animals can detect a behaviorally-relevant stimulus change (Womelsdorf et al., 2006). EEG studies in humans provide convergent evidence that

pre-stimulus fluctuations in phase coupling can modulate target detection (Hanslmayr et al., 2007). Furthermore, intrinsic fluctuations of phase coupling are associated with fluctuations in perceptual states in ambiguous stimulus settings. Fluctuations in beta-band or gamma-band phase coupling have been shown to predict the perceptual state in ambiguous sensory paradigms (Hipp et al., 2011; Rose and Büchel, 2005) and decision making in near-threshold stimulation regimes (Donner et al., 2009). Our current results corroborate and extend this evidence by showing that, at perceptual threshold, detection of the lateralized stimuli by the animals is biased by phase coupling in the pre-stimulus interval.

A crucial element in our approach is the ability to simultaneously monitor numerous cortical areas, enabling us to quantify within-system and between-system interactions and to characterize these in a spectrally resolved manner. Our analysis showed that, in particular, long-range connectivity between different functional systems was related to successful stimulus detection. This is in line with the hypothesis that long-range phase coupling may serve efficient transmission of task-relevant information in sensorimotor networks (Engel et al., 2001; Fries, 2005; Womelsdorf et al., 2007). One important finding was that the variations in connectivity patterns associated to changes in behavioral performances, do not occur arbitrarily along the whole cortex, but in specific subnetworks, which were identified by extracting principal components of functional connectivity. Whether these subnetworks are associated to a decision making network, or rather sensory processing is not clear. However, since most of the nodes include primary sensory areas, and the connectivity changes occurred before the stimulus was presented, we speculate that the first reason for miss trials is a sub-optimal function of stimulus coding.

Our results also support the view that the characterization of changes in brain-state strongly benefits from inclusion of connectivity analyses. The observation that changes in network state are reflected, in particular, in fluctuations of large-scale connectivity, is in line with results of other recent studies. In rats (Olcese et al., 2016) has being shown that functional connectivity within and between brain areas is modulated across behavioral states in a region-specific manner. Supportive evidence has been obtained in studies on the human brain (He et al., 2008; Supp et al., 2011). Using the same ECoG recording approach for the study of ongoing activity, we have observed that functional connectivity shows state-dependent reconfiguration which can also involve shifts in the ratio between short- and long-range interactions (Stitt et al., 2017; Fischer et al., 2018). These findings raise the question of possible mechanisms that might modulate large-scale functional connectivity in a state- and task-dependent manner. Possible candidates are changes in the output of ascending neuromodulatory systems (Harris and Thiele, 2011). Phase coupling has long been known to be influenced by neuromodulators (Steriade et al., 1993). For instance, activation of cholinergic brain stem nuclei has been shown to enhance gamma-band phase coupling in cortical networks (Munk et al., 1996). Neuropharmacological evidence suggests, furthermore, that noradrenergic brain stem inputs can modulate large-scale functional connectivity in cortex (van den Brink et al., 2018).

Finally, while the use of ferrets as a model in neuroscience is gaining interest in research, the limitations in sample size remain a constraint for statistical analysis. Factors in our preparation that may be bolstered by small sample sizes include the variability of cortical structure across animals, which may, for instance, lead to different numbers of electrodes per cortical area, or differences between recording sessions in the same animal. To address this limitation, we pooled data from all animals and recording sessions to improve our statistical conclusions and discarded short sessions where the animal's motivation was not present. Secondly, we employed a detection task to measure the connectivity between distant cortical areas. However, we cannot ignore the fact that neural activity and functional connectivity can be modulated by attention or top-down effects. We acknowledge that with our recording setup, we were unable to measure top-down contributions or levels of attention. Two possibilities to address this in the future would be to record activity in the frontal cortex and to use an additional biomarker to quantify attention, such as pupillometry. This issue is not minor, as top-down signals can modify primary areas (e.g., A1 and V1) by introducing common inputs, potentially leading to apparent connectivity that does not actually exist. This problem cannot be completely eliminated even by excluding zero-phase correlations (e.g., with imaginary coherence) or using causality measures. To definitively rule out common source artifacts, it would be necessary to directly manipulate one of the pathways, for instance through lesion or inactivation, but this is currently not part of our approach.

Conclusion

Our study has demonstrated functional coupling across visual, auditory and parietal areas during a lateralized detection task in the ferret. Analysis of power for hit and miss trials revealed significant differences around stimulus and response onset. In contrast, phase coupling already differed between hits and misses at baseline, suggesting an essential role of large-scale functional connectivity in the animal's ability to perform the task. In particular, higher phase coupling of visual and auditory regions to parietal cortex was predictive of task performance. We observed that long-range coupling became more predominant during the task period compared to the pre-stimulus baseline. Taken together, these results suggest that fluctuations in the network state, particularly with respect to long-range connectivity, are critical determinants of the animals' behavior. Future studies might address the relation to the underlying structural connectivity and the mechanisms that give rise to the observed variability of phase coupling.

Data availability statement

The results data supporting the conclusions of this article will be made available by the authors, without undue reservation.

Ethics statement

The animal study was approved by Hamburg state authority for animal welfare (BUG-Hamburg). The study was conducted in accordance with the local legislation and institutional requirements.

Author contributions

EG-L: Conceptualization, Formal analysis, Investigation, Visualization, Writing – original draft, Writing – review & editing. KH:

Conceptualization, Data curation, Formal analysis, Investigation, Methodology, Visualization, Writing – original draft, Writing – review & editing. FP: Data curation, Resources, Software, Writing – review & editing. GE: Investigation, Project administration, Resources, Supervision, Writing – review & editing. GN: Conceptualization, Software, Writing – review & editing. AKE: Conceptualization, Funding acquisition, Resources, Supervision, Visualization, Writing – review & editing.

Conflict of interest

The authors declare that the research was conducted in the absence of any commercial or financial relationships that could be construed as a potential conflict of interest.

Generative AI statement

The authors declare that no Gen AI was used in the creation of this manuscript.

Publisher's note

All claims expressed in this article are solely those of the authors and do not necessarily represent those of their affiliated organizations, or those of the publisher, the editors and the reviewers. Any product that may be evaluated in this article, or claim that may be made by its manufacturer, is not guaranteed or endorsed by the publisher.

Author disclaimer

The views and opinions expressed in this paper are those of the authors only and do not necessarily reflect those of the European Union or the European Research Council. Neither the European Union nor the granting authority can be held responsible for them.

Supplementary material

The Supplementary material for this article can be found online at: https://www.frontiersin.org/articles/10.3389/fnsys.2025.1524547/full#supplementary-material

References

Alais, D., Newell, F., and Mamassian, P. (2010). Multisensory processing in review: from physiology to behaviour. *Seeing Perceiving* 23, 3–38. doi: 10.1163/187847510X488603

Arieli, A., Sterkin, A., Grinvald, A., and Aertsen, A. (1996). Dynamics of ongoing activity: explanation of the large variability in evoked cortical responses. *Science* 273, 1868–1871. doi: 10.1126/science.273.5283.1868

Arnal, L. H., Poeppel, D., and Giraud, A. (2015). Temporal coding in the auditory cortex. *Handb. Clin. Neurol.* 129, 85–98. doi: 10.1016/B978-0-444-62630-1.00005-6

Baratham, V. L., Dougherty, M. E., Hermiz, J., Ledochowitsch, P., Maharbiz, M. M., and Bouchard, K. E. (2022). Columnar localization and laminar origin of cortical surface electrical poten tials. *J. Neurosci.* 42, 3733–3748. doi: 10.1523/JNEUROSCI.1787-21.2022

Bastos, A. M., Usrey, W. M., Adams, R. A., Mangun, G. R., Fries, P., and Friston, K. J. (2012). Canonical microcircuits for predictive coding. *Neuron* 76, 695–711. doi: 10.1016/j.neuron.2012.10.038

Bastos, A. M., Vezoli, J., Bosman, C. A., Schoffelen, J. M., Oostenveld, R., Dowdall, J. R., et al. (2015). Visual areas exert feedforward and feedback influences through distinct frequency channels. *Neuron* 85, 390–401. doi: 10.1016/j.neuron.2014.12.018

Bernasconi, C., von Stein, A., Chiang, C., and König, P. (2000). Bi-directional interactions between visual areas in the awake behaving cat. *Neuroreport* 11, 689–692. doi: 10.1097/00001756-200003200-00007

Bizley, J. K., Bajo, V. M., Nodal, F. R., and King, A. J. (2015). Cortico-cortical connectivity within ferret auditory cortex. *J. Comp. Neurol.* 523, 2187–2210. doi: 10.1002/cne.23784

Bizley, J., Nodal, F., Bajo, V., Nelken, I., and King, A. (2007). Physiological and anatomical evidence for multisensory interactions in auditory cortex. *Cereb. Cortex* 17, 2172–2189. doi: 10.1093/cercor/bhl128

Bockhorst, T., Pieper, F., Engler, G., Stieglitz, T., Galindo-Leon, E., and Engel, A. K. (2018). Synchrony surfacing: epicortical recording of correlated action potentials. *Eur. J. Neurosci.* 48, 3583–3596. doi: 10.1111/ejn.14167

Bosman, C. A., Schoffelen, J. M., Brunet, N., Oostenveld, R., Bastos, A. M., Womelsdorf, T., et al. (2012). Attentional stimulus selection through selective synchronization between monkey visual areas. *Neuron* 75, 875–888. doi: 10.1016/j.neuron.2012.06.037

Brainard, D. H. (1997). The psychophysics toolbox. *Spat. Vis.* 10, 433–436. doi: 10.1163/156856897X00357

Brookes, M. J., Hale, J. R., Zumer, J. M., Stevenson, C. M., Francis, S. T., Barnes, G. R., et al. (2011). Measuring functional connectivity using MEG: methodology and comparison with fcMRI. *NeuroImage* 56, 1082–1104. doi: 10.1016/j.neuroimage.2011.02.054

Busch, N. A., Dubois, J., and VanRullen, R. (2009). The phase of ongoing EEG oscillations predicts visual perception. *J. Neurosci.* 29, 7869–7876. doi: 10.1523/JNEUROSCI.0113-09.2009

Buzsaki, G. (2006). Rhythms of the brain. Oxford: Oxford University Press.

Canolty, R., and Knight, R. (2010). The functional role of cross-frequency coupling. *Trends Cogn. Sci.* 14, 506–515. doi: 10.1016/j.tics.2010.09.001

Coulter, D. A., Yue, C., Ang, C. W., Weissinger, F., Goldberg, E., Hsu, F. C., et al. (2011). Hippocampal microcircuit dynamics probed using optical imaging approaches. *J. Physiol.* 589, 1893–1903. doi: 10.1113/jphysiol.2010.202184

Crone, N. E., Sinai, A., and Korzeniewska, A. (2006). High-frequency gamma oscillations and human brain mapping with electrocorticography. *Prog. Brain Res.* 159, 275–295. doi: 10.1016/S0079-6123(06)59019-3

Donner, T. H., Siegel, M., Fries, P., and Engel, A. K. (2009). Buildup of choice-predictive activity in human motor cortex during perceptual decision making. *Curr. Biol.* 19, 1581–1585. doi: 10.1016/j.cub.2009.07.066

Engel, A. K., and Fries, P. (2010). Beta-band oscillations—signalling the status quo? *Curr. Opin. Neurobiol.* 20, 156–165. doi: 10.1016/j.conb.2010.02.015

Engel, A. K., Fries, P., and Singer, W. (2001). Dynamic predictions: oscillations and synchrony in top-down processing. *Nat. Rev. Neurosci.* 2, 704–716. doi: 10.1038/35094565

Engel, A., Gerloff, C., Hilgetag, C., and Nolte, G. (2013). Intrinsic coupling modes: multiscale interactions in ongoing brain activity. *Neuron* 80, 867–886. doi: 10.1016/j.neuron.2013.09.038

Feldmeyer, D., Brecht, M., Helmchen, F., Petersen, C. C. H., Poulet, J. F. A., Staiger, J. F., et al. (2013). Barrel cortex function. *Prog. Neurobiol.* 103, 3–27. doi: 10.1016/j.pneurobio.2012.11.002

Fischer, F., Pieper, F., Galindo-Leon, E., Engler, G., Hilgetag, C. C., and Engel, A. K. (2018). Intrinsic functional connectivity resembles cortical architecture at various levels of isoflurane anesthesia. *Cereb. Cortex* 28, 2991–3003. doi: 10.1093/cercor/bhy114

Fox, K. C. R., Foster, B. L., Kucyi, A., Daitch, A. L., and Parvizi, J. (2018). Intracranial electrophysiology of the human default network. *Trends Cogn. Sci.* 22, 307–324. doi: 10.1016/j.tics.2018.02.002

Fries, P. (2005). A mechanism for cognitive dynamics: neuronal communication through neuronal coherence. *Trends Cogn. Sci.* 9, 474–480. doi: 10.1016/j.tics.2005.08.011

Fries, P., Neuenschwander, S., Engel, A. K., Goebel, R., and Singer, W. (2001). Rapid feature selective neuronal synchronization through correlated latency shifting. *Nat. Neurosci.* 4, 194–200. doi: 10.1038/84032

Fukushima, M., Chao, Z. C., and Fujii, N. (2015). Studying brain functions with mesoscopic measurements: advances in electrocorticography for non-human primates. *Curr. Opin. Neurobiol.* 32, 124–131. doi: 10.1016/j.conb.2015.03.015

Galindo-Leon, E., Stitt, I., Pieper, F., Stieglitz, T., Engler, G., and Engel, A. K. (2019). Context-specific modulation of intrinsic coupling modes shapes multisensory processing. *Sci. Adv.* 5:eaar7633. doi: 10.1126/sciadv.aar7633

Ghazanfar, A. A., Chandrasekaran, C., and Logothetis, N. K. (2008). Interactions between the superior temporal sulcus and auditory cortex mediate dynamic face/voice integration in rhesus monkeys. *J. Neurosci.* 28, 4457–4469. doi: 10.1523/JNEUROSCI.0541-08.2008

Giordano, B. L., Ince, R. A. A., Gross, J., Schyns, P. G., Panzeri, S., and Kayser, C. (2017). Contributions of local speech encoding and functional connectivity to audio-visual speech perception. *eLife* 6:e24763. doi: 10.7554/eLife.24763

Giraud, A.-L., and Poeppel, D. (2012). Cortical oscillations and speech processing: emerging computational principles and operations. *Nat. Neurosci.* 15, 511–517. doi: 10.1038/nn.3063

Green, A. M., and Angelaki, D. E. (2010). Multisensory integration: resolving sensory ambiguities to build novel representations. *Curr. Opin. Neurobiol.* 20, 353–360. doi: 10.1016/j.conb.2010.04.009

Gregoriou, G. G., Gotts, S. J., Zhou, H., and Desimone, R. (2009). High-frequency, long-range coupling between prefrontal and visual cortex during attention. *Science* 324, 1207–1210. doi: 10.1126/science.1171402

Hanslmayr, S., Aslan, A., Staudigl, T., Klimesch, W., Herrmann, C. S., and Bäuml, K. H. (2007). Prestimulus oscillations predict visual perception performance between and within subjects. *NeuroImage* 37, 1465–1473. doi: 10.1016/j.neuroimage.2007.07.011

Harris, K. D., and Thiele, A. (2011). Cortical state and attention. *Nat. Rev. Neurosci.* 12, 509–523. doi: 10.1038/nrn3084

He, B. J., Snyder, A. Z., Zempel, J. M., Smyth, M. D., and Raichle, M. E. (2008). Electrophysiological correlates of the brain's intrinsic large-scale functional architecture. *Proc. Natl. Acad. Sci. U.S.A.* 105, 16039–16044. doi: 10.1073/pnas.0807010105

Hipp, J. F., Engel, A. K., and Siegel, M. (2011). Oscillatory synchronization in large-scale cortical networks predicts perception. *Neuron* 69, 387–396. doi: 10.1016/j.neuron.2010.12.027

Hollensteiner, K. J., Pieper, F., Engler, G., König, P., and Engel, A. K. (2015). Crossmodal integration improves sensory detection thresholds in the ferret. *PLoS One* 10:e0124952. doi: 10.1371/journal.pone.0124952

Hyvärinen, A., and Oja, E. (2000). Independent component analysis: algorithms and applications. *Neural Netw.* 13, 411–430. doi: 10.1016/S0893-6080(00)00026-5

Jensen, O., and Mazaheri, A. (2010). Shaping functional architecture by oscillatory alpha activity: gating by inhibition. *Front. Hum. Neurosci.* 4:186. doi: 10.3389/fnhum.2010.00186

Kaernbach, C. (1991). Simple adaptive testing with the weighted up-down method. *Percept. Psychophys.* 49, 227–229. doi: 10.3758/BF03214307

Kayser, C., Petkov, C. I., and Logothetis, N. K. (2008). Visual modulation of neurons in auditory cortex. *Cereb. Cortex* 18, 1560–1574. doi: 10.1093/cercor/bhm187

Keil, J., Müller, N., Hartmann, T., and Weisz, N. (2014). Prestimulus beta power and phase synchrony influence the sound-induced flash illusion. *Cereb. Cortex* 24, 1278–1288. doi: 10.1093/cercor/bhs409

Keller, C. J., Honey, C. J., Mégevand, P., Entz, L., Ulbert, I., and Mehta, A. D. (2014). Mapping human brain networks with cortico-cortical evoked potentials. *Philos. Trans. R. Soc. B* 369:20130528. doi: 10.1098/rstb.2013.0528

Lachaux, J., Rodriguez, E., Martinerie, J., and Varela, F. (1999). Measuring phase synchrony in brain signals. *Hum. Brain Mapp.* 8, 194–208. doi: 10.1002/(SICI)1097-0193(1999)8:4<194::AID-HBM4>3.0.CO;2-C

Lakatos, P., Chen, C.-M., O'Connell, M. N., Mills, A., and Schroeder, C. E. (2007). Neuronal oscillations and multisensory interaction in primary auditory cortex. *Neuron* 53, 279–292. doi: 10.1016/j.neuron.2006.12.011

Leonardi, N., Richiardi, J., Gschwind, M., Simioni, S., Annoni, J. M., Schluep, M., et al. (2013). Principal components of functional connectivity: a new approach to study dynamic brain connectivity during rest. *NeuroImage* 83, 937–950. doi: 10.1016/j.neuroimage.2013.07.019

Lewis, C., Bosman, C., and Fries, P. (2015). Recording of brain activity across spatial scales. *Curr. Opin. Neurobiol.* 32, 68–77. doi: 10.1016/j.conb.2014.12.007

Liebe, S., Hoerzer, G. M., Logothetis, N. K., and Rainer, G. (2012). Theta coupling between V4 and prefrontal cortex predicts visual short-term memory performance. *Nat. Neurosci.* 15, 456–462. doi: 10.1038/nn.3038

Lima, B., Singer, W., and Neuenschwander, S. (2011). Gamma responses correlate with temporal expectation in monkey primary visual cortex. *J. Neurosci.* 31, 15919–15931. doi: 10.1523/JNEUROSCI.0957-11.2011

Maier, J. X., Chandrasekaran, C., and Ghazanfar, A. A. (2008). Integration of bimodal looming signals through neuronal coherence in the temporal lobe. *Curr. Biol.* 18, 963–968. doi: 10.1016/j.cub.2008.05.043

Michalareas, G., Vezoli, J., van Pelt, S., Schoffelen, J. M., Kennedy, H., and Fries, P. (2016). Alpha-beta and gamma rhythms subserve feedback and feedforward influences among human visual cortical areas. *Neuron* 89, 384–397. doi: 10.1016/j.neuron.2015.12.018

Miller, E. K., and Buschman, T. J. (2013). Cortical circuits for the control of attention. *Curr. Opin. Neurobiol.* 23, 216–222. doi: 10.1016/j.conb.2012.11.011

Munk, M. H. J., Roelfsema, P. R., König, P., Engel, A. K., and Singer, W. (1996). Role of reticular activation in the modulation of intracortical synchronization. *Science* 272, 271–274. doi: 10.1126/science.272.5259.271

Nodal, F. R., Bajo, V. M., Parsons, C. H., Schnupp, J. W., and King, A. J. (2008). Sound localization behavior in ferrets: comparison of acoustic orientation and approach-to-target responses. *Neuroscience* 154, 397–408. doi: 10.1016/j.neuroscience.2007.12.022

Nolte, G., Ziehe, A., Nikulin, V. V., Schlögl, A., Krämer, N., Brismar, T., et al. (2008). Robustly estimating the flow direction of information in complex physical systems. *Phys. Rev. Lett.* 100:234101. doi: 10.1103/PhysRevLett.100.234101

Olcese, U., Bos, J. J., Vinck, M., Lankelma, J. V., van Mourik-Donga, L. B., Schlumm, F., et al. (2016). Spike-based functional connectivity in cerebral cortex and hippocampus: loss of global connectivity is coupled to preservation of local connectivity during non-REM sleep. *J. Neurosci.* 36, 7676–7692. doi: 10.1523/JNEUROSCI.4201-15.2016

Ploner, M., Sorg, C., and Gross, J. (2017). Brain rhythms of pain. *Trends Cogn. Sci.* 21, 100–110. doi: 10.1016/j.tics.2016.12.001

Proháczik, A., Kulcsár, M., Trigg, T., Driancourt, M. A., and Huszenicza, G. (2010). Comparison of four treatments to suppress ovarian activity in ferrets (*Mustela putorius furo*). *Vet. Rec.* 166, 74–78. doi: 10.1136/vr.c177

Raichle, M. E. (2010). Two views of brain function. *Trends Cogn. Sci.* 14, 180–190. doi: 10.1016/j.tics.2010.01.008

Roelfsema, P. R., Engel, A. K., König, P., and Singer, W. (1997). Visuomotor integration is associated with zero time-lag synchronization among cortical areas. *Nature* 385, 157–161. doi: 10.1038/385157a0

Rose, M., and Büchel, C. (2005). Neural coupling binds visual tokens to moving stimuli. *J. Neurosci.* 25, 10101–10104. doi: 10.1523/JNEUROSCI.2998-05.2005

Rubehn, B., Bosman, C., Oostenveld, R., Fries, P., and Stieglitz, T. (2009). A MEMS-based flexible multichannel ECoG-electrode array. *J. Neural Eng.* 6:036003. doi: 10.1088/1741-2560/6/3/036003

Saalmann, Y. B., Pinsk, M. A., Wang, L., Li, X., and Kastner, S. (2012). The pulvinar regulates information transmission between cortical areas based on attention demands. *Science* 337, 753–756. doi: 10.1126/science.1223082

Salazar, R. F., Dotson, N. M., Bressler, S. L., and Gray, C. M. (2012). Content-specific fronto-parietal synchronization during visual working memory. *Science* 338, 1097–1100. doi: 10.1126/science.1224000

Senkowski, D., Schneider, T. R., Foxe, J. J., and Engel, A. K. (2008). Crossmodal binding through neural coherence: implications for multisensory processing. *Trends Neurosci.* 31, 401–409. doi: 10.1016/j.tins.2008.05.002

Shadlen, M., Britten, K., Newsome, W., and Movshon, J. (1996). A computational analysis of the relationship between neuronal and behavioral responses to visual motion. *J. Neurosci.* 16, 1486–1510. doi: 10.1523/JNEUROSCI.16-04-01486.1996

Siegel, M., Donner, T. H., and Engel, A. K. (2012). Spectral fingerprints of large-scale neuronal interactions. *Nat. Rev. Neurosci.* 13, 121–134. doi: 10.1038/nrn3137

Siegel, M., Donner, T. H., Oostenveld, R., Fries, P., and Engel, A. K. (2008). Neuronal synchronization along the dorsal visual pathway reflects the focus of spatial attention. *Neuron* 60, 709–719. doi: 10.1016/j.neuron.2008.09.010

Singer, W., and Gray, C. M. (1995). Visual feature integration and the temporal correlation hypothesis. *Annu. Rev. Neurosci.* 18, 555–586. doi: 10.1146/annurev.ne.18.030195.003011

Stein, B., and Meredith, M. (1993). The merging of the senses. Cambridge, MA: MIT Press.

Steriade, M., Contreras, D., Amzica, F., and Timofeev, I. (1996). Synchronization of fast (30–40 Hz) spontaneous oscillations in intrathalamic and thalamocortical networks. *J. Neurosci.* 16, 2788–2808. doi: 10.1523/JNEUROSCI.16-08-02788.1996

Steriade, M., McCormick, D. A., and Sejnowski, T. J. (1993). Thalamocortical oscillations in the sleeping and aroused brain. *Science* 262, 679–685. doi: 10.1126/science.8235588

Stitt, I., Hollensteiner, K. J., Galindo-Leon, E., Pieper, F., Fiedler, E., Stieglitz, T., et al. (2017). Dynamic reconfiguration of cortical functional connectivity across brain states. *Sci. Rep.* 7:8797. doi: 10.1038/s41598-017-08050-6

Supp, G. G., Siegel, M., Hipp, J. F., and Engel, A. K. (2011). Cortical hypersynchrony predicts breakdown of sensory processing during loss of consciousness. *Curr. Biol.* 21, 1988–1993. doi: 10.1016/j.cub.2011.10.017

Talsma, D., Senkowski, D., Soto-Faraco, S., and Woldorff, M. G. (2010). The multifaceted interplay between attention and multisensory integration. *Trends Cogn. Sci.* 14, 400–410. doi: 10.1016/j.tics.2010.06.008

Toda, H., Kawasaki, K., Sato, S., Horie, M., Nakahara, K., Bepari, A. K., et al. (2018). Locally induced neuronal synchrony precisely propagates to specific cortical areas without rhythm distortion. *Sci. Rep.* 8:7678. doi: 10.1038/s41598-018-26054-8

van Atteveldt, N., Murray, M. M., Thut, G., and Schroeder, C. E. (2014). Multisensory integration: flexible use of general operations. *Neuron* 81, 1240–1253. doi: 10.1016/j.neuron.2014.02.044

van den Brink, R. L., Nieuwenhuis, S., and Donner, T. H. (2018). Amplification and suppression of distinct brainwide activity patterns by catecholamines. *J. Neurosci.* 38, 7476–7491. doi: 10.1523/JNEUROSCI.0514-18.2018

Varela, F., Lachaux, J.-P., Rodriguez, E., and Martinerie, J. (2001). The brainweb: phase synchronization and large-scale integration. *Nat. Rev. Neurosci.* 2, 229–239. doi: 10.1038/35067550

Wang, P., Göschl, F., Friese, U., König, P., and Engel, A. K. (2019). Long-range functional coupling predicts performance: oscillatory EEG networks in multisensory processing. *NeuroImage* 196, 114–125. doi: 10.1016/j.neuroimage.2019.04.001

Womelsdorf, T., and Fries, P. (2007). The role of neuronal synchronization in selective attention. *Curr. Opin. Neurobiol.* 17, 154–160. doi: 10.1016/j.conb.2007.02.002

Womelsdorf, T., Fries, P., Mitra, P. P., and Desimone, R. (2006). Gamma-band synchronization in visual cortex predicts speed of change detection. *Nature* 439, 733–736. doi: 10.1038/nature04258

Womelsdorf, T., Schoffelen, J. M., Oostenveld, R., Singer, W., Desimone, R., Engel, A. K., et al. (2007). Modulation of neuronal interactions through neuronal synchronization. *Science* 316, 1609–1612. doi: 10.1126/science.1139597

Zohary, E., Shadlen, M. N., and Newsome, W. T. (1994). Correlated neuronal discharge rate and its implications for psychophysical performance. *Nature* 370, 140–143. doi: 10.1038/370140a0